ISSN 1998-0124 CN 11-5974/O4
https://doi.org/10.26599/NR.2025.94907052

Research Article

Dynamically self-adjustable liquid-liquid and self-adaptive soft-contact solid-solid triboelectric nanogenerator for wave energy harvesting

Yong Long[1,2,§], Bingqi Zhao[2,3,§], Jianan Niu[2,3], Yuxiu Liu[2,3], Wei Sha[2,3], Jiangwen Wang[2,3], Zhong Lin Wang[1,2,3](✉), Weiguo Hu[1,2,3](✉)

[1] Guangzhou Institute of Blue Energy, Knowledge City, Huangpu District, Guangzhou 510555, China

[2] Beijing Institute of Nanoenergy and Nanosystems, Chinese Academy of Sciences, Beijing 101400, China

[3] School of Nanoscience and Technology, University of Chinese Academy of Sciences, Beijing 100049, China

[§] Yong Long and Bingqi Zhao contributed equally to this work.

Nano Res., **Just Accepted Manuscript** • https://doi.org/10.26599/NR.2025.94907052
https://www.sciopen.com/journal/1998-0124 on Sep. 25, 2024

TABLE OF CONTENTS (TOC)

Dynamically self-adjustable liquid-liquid and self-adaptive soft-contact solid-solid triboelectric nanogenerator for wave energy harvesting

Yong Long[1,2,§], Bingqi Zhao[2,3,§], Jianan Niu[2,3], Yuxiu Liu[2,3], Wei Sha[2,3], Jiangwen Wang[2,3], Zhong Lin Wang[1,2,3*], Weiguo Hu[1,2,3*]

[1] Guangzhou Institute of Blue Energy, Knowledge City, Huangpu District, Guangzhou 510555, China

[2] Beijing Institute of Nanoenergy and Nanosystems, Chinese Academy of Sciences, Beijing 101400, China

[3] School of Nanoscience and Technology, University of Chinese Academy of Sciences, Beijing 100049, China

[§] Yong Long and Bingqi Zhao contributed equally to this work.

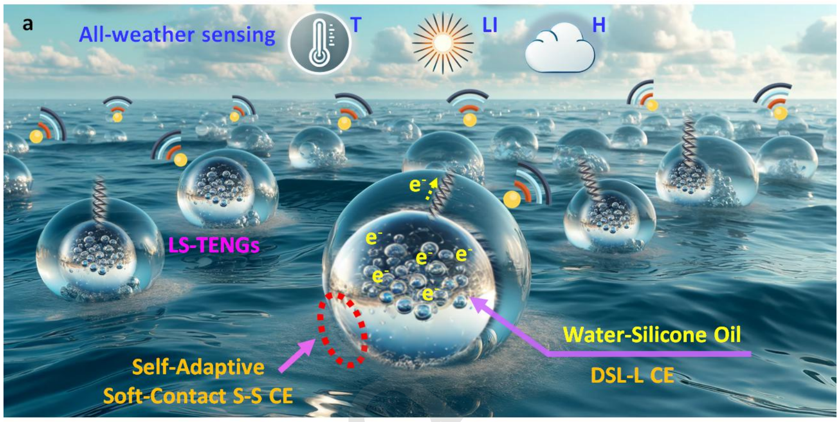

The paper presents a novel ellipsoidal, pendulum-like triboelectric nanogenerator (LS-TENG) that integrates both liquid-liquid (L-L) and solid-solid (S-S) triboelectric effects, designed for efficient wave energy harvesting and continuous, self-powered marine environment monitoring. The innovative structure, with dynamically self-adjustable L-L interfaces and self-adaptive soft S-S contacts, significantly enhances energy harvesting efficiency and protects the device from mechanical wear, offering a promising solution for sustainable energy generation in marine environments.

Nano Research

ISSN 1998-0124 CN 11-5974/O4
https://doi.org/10.26599/NR.2025.94907052

Research Article

Dynamically self-adjustable liquid-liquid and self-adaptive soft-contact solid-solid triboelectric nanogenerator for wave energy harvesting

Yong Long[1,2,§], Bingqi Zhao[2,3,§], Jianan Niu[2,3], Yuxiu Liu[2,3], Wei Sha[2,3], Jiangwen Wang[2,3], Zhong Lin Wang[1,2,3] (✉), and Weiguo Hu[1,2,3] (✉)

[1] Guangzhou Institute of Blue Energy, Knowledge City, Huangpu District, Guangzhou 510555, China
[2] Beijing Institute of Nanoenergy and Nanosystems, Chinese Academy of Sciences, Beijing 101400, China
[3] School of Nanoscience and Technology, University of Chinese Academy of Sciences, Beijing 100049, China
[§] Yong Long and Bingqi Zhao contributed equally to this work.

Received: 12 August 2024 / **Revised:** 24 September 2024 / **Accepted:** 25 September 2024

ABSTRACT

Water wave energy exhibits great potential to alleviate the global energy crisis. However, harvesting and utilizing wave energy are challenging due to its irregularity, randomness, and low frequency. Triboelectric nanogenerators (TENGs) have gained significant attention for harvesting wave energy with high efficiency. This study presents a novel ellipsoidal, pendulum-like TENG integrating both liquid-liquid (L-L) and solid-solid (S-S) triboelectricity (LS-TENG). This innovative design enables continuous wave energy harvesting and self-powered marine environment monitoring under various conditions, including temperature, humidity, and light intensity. The binary immiscible liquids within the LS-TENG's inner soft balloon create dynamic, and self-adjustable L-L contact interfaces, significantly increasing the L-L contact area and enhancing L-L contact electrification (CE). The unique self-adaptive, soft S-S contact increases the S-S contact area compared to traditional hard point contact, better adapting to the irregular movements of waves and promoting efficient S-S CE. The LS-TENG achieves highly efficient wave energy harvesting by coupling L-L and S-S CE. Furthermore, the unique soft contact design protects the S-S interfaces from mechanical wear and damage during long-term work. The LS-TENG's novel structure provides an innovative and effective way for water wave energy harvesting.

KEYWORDS

self-adaptive, soft-contact, solid-solid, liquid-liquid, self-adjustable, triboelectric nanogenerator

1 Introduction

The escalating global energy demand and the environmental influence of traditional fossil fuels have intensified the search for sustainable and renewable energy sources [1-3]. Among the various renewable energy options, water wave energy, as a clean and inexhaustible energy resource, stands out due to its inherent characteristic of being abundant, predictable, and consistent, which can alleviate the global energy crisis [2, 4-9]. However, despite its potential, effectively harvesting and harnessing wave energy remains a challenge. This is primarily due to unresolved technological issues and the high costs associated with energy harvesting. Additionally, the irregular and low-frequency nature of ocean waves complicates the energy conversion process, making it difficult to capture energy efficiently [2, 5, 10-14].

Triboelectric nanogenerators (TENGs) [10-13, 15], based on the expanded Maxwell's displacement current as the underlying physical mechanism and with the polarization density term P_S in the electrical displacement vector as its central element [16, 17], have emerged as a novel solution to these challenges which are mainly employed to harvest energy from irregular and low-frequency mechanical motions, consequently well-suitable for ocean wave energy harvesting [12, 18-27]. Although recent progress based on new materials and novel TENG devices, even including artificial intelligence (AI) for future TENG materials and devices, is emerging [28-32], traditional TENGs designed for water wave harvesting are typically spherical structures that utilize rigid S-S point contact [33-38]. This type of configuration still results in several problems, such as limited point contact areas and insufficient contact-separation dynamics, leading to inefficient energy harvesting [37]. Besides, the physical structure of these spherical TENGs is always too complicated to fabricate, and the adaptability of the internal parts to water wave motions is quite limited [1, 26, 39-42]. More importantly, the S-S interface's hard contact can easily cause mechanical wear and potentially damage the TENG devices, leading to water leakage. Additionally, these issues seriously hinder the practical application and longevity of TENGs in marine environments [38, 43-47].

To address the above problems of conventional TENGs for water wave energy harvesting, in this study, we design a novel ellipsoidal and pendulum-like structured TENG that integrates both L-L and S-S contact electrification (CE) (LS-TENG), enabling continuous harvesting of wave energy and self-powered monitoring of the marine environment under all weather conditions, including temperature (T), humidity (H),

Address correspondence to Weiguo Hu, huweiguo@binn.cas.cn; Zhong Lin Wang, zlwang@binn.cas.cn

and light intensity (LI) (Figure 1a). The structure of the LS-TENG mainly consisted of the outermost hard spherical shell and the internal cotton-covered soft liquid balloon system, which is hung and balanced in the liquid balloon's inner chamber via a copper core spring (Cu-spring), and takes on an ellipsoidal shape due to gravity (Figure 1b). In the balloon, two kinds of immiscible liquid were injected as the binary liquid electrodes. This innovative structural design integrated both L-L and S-S interface triboelectric effects during the LS-TENG's working process to significantly enhance the wave energy harvesting efficiency.

The soft liquid balloon adapts dynamically to the irregular motions of water waves, enabling a unique self-adaptive and soft contact with the inner surface of the external hard spherical shell. This adaptation significantly increases the S-S contact area [37], which can not only boost energy harvesting efficiency but also play a crucial role in reducing mechanical wear and extending the TENG's operational lifespan. The introduced immiscible binary liquid electrodes in the inner soft balloon create large numbers of dynamic self-adjustable L-L contact interfaces when driven by the movement of water waves, significantly increasing the L-L contact area, thus promoting the transfer of triboelectric charge generated between L-L interfaces and enhancing the efficiency of wave energy harvesting (Figure 1c) [17, 48, 49]. Besides, this spring-driven approach provides a quick and thorough S-S contact-separation process and effectively facilitates the separation of generated triboelectric charges, promoting wave energy harvesting efficiency. Furthermore, we reasonably proposed the triboelectric charge transfer mechanism at the dynamic self-adjustable L-L contact interface by comparing the LS-TENG's output performances based on different kinds of immiscible binary liquid electrode systems. Additionally, by enabling the LS-TENG to continuously harvest water wave energy, self-powered monitoring of marine environments under all weather conditions is successfully realized, demonstrating the LS-TENG's promising potential in harvesting and utilizing wave energy. The development of the LS-TENG represents a significant advance in wave energy harvesting.

2. Results and Discussion

2.1 Structure of the LS-TENG.

The structure of the fabricated LS-TENG mainly consists of two parts: an external transparent hard acrylic spherical shell and an internal soft liquid latex balloon covered with a cotton layer (Figure 1b). Regarding the external acrylic spherical shell, a layer of silver, acting as one of the electrodes, was coated on the inner surface of the hard acrylic spherical shell by magnetron sputtering. Then, a polyimide tape is adhered to this silver layer to serve as a dielectric layer. The optical image of the device shows the silver layer uniformly coated on the inner surface of the acrylic shell (Figure S1). As for the second part, the preparation process of the internal soft liquid balloon can be seen visually in Figure S2. Firstly, a copper core spring is inserted into the latex balloon. Then two kinds of immiscible liquids, silicone oil and deionized water, are injected into the balloon as the binary liquid electrodes to make the balloon bulge. Then, a thin cotton layer covers the outside of the liquid balloon to serve as one of the S-S contact interfaces. The entire liquid balloon system is securely suspended within the inner cavity of the external hard acrylic spherical shell through the copper core spring, which not only can transport the L-L triboelectric charges but also allows for the adaptive and responsive movement of the internal soft liquid balloon system inside the hard spherical shell. The other end of the copper core spring passes through the tiny hole in the rigid acrylic ball shell to connect with the external circuit.

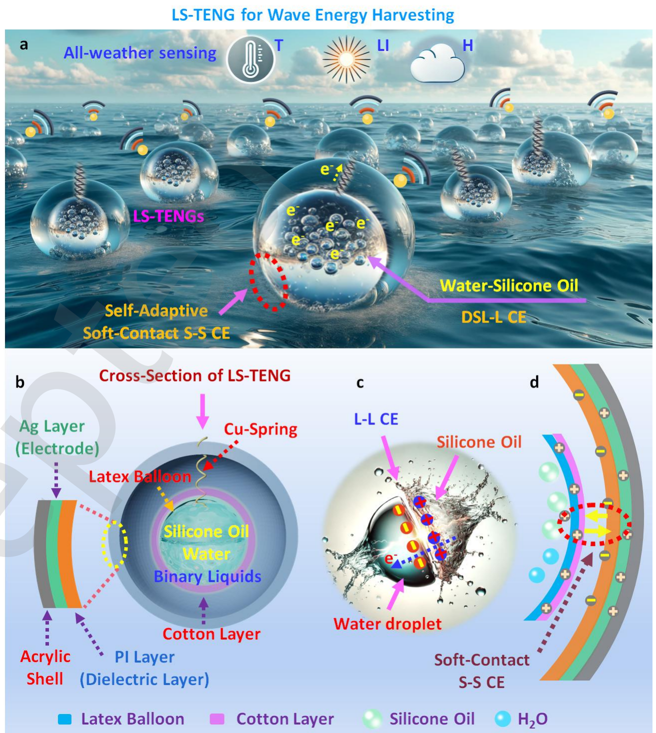

Figure 1. Wave energy harvesting and marine environment monitoring used by the LS-TENG and its structure and fabrication process. a) The wave energy harvesting and continuously self-powered all-weather monitoring of marine environments, including temperature (T), light intensity (LI) and humidity (H). b) Cross-section of the LS-TENG showing its interior structural details. c) The transfer of triboelectric charge generated between the L-L interfaces. d) The unique self-adaptive and soft contact manner between the S-S contact interfaces.

The inner soft liquid balloon, the key component of our LS-TENG, is fabricated from a commercial latex balloon that is robust, elastic, flexible, and chemically stable. These inherent advantages are vital for facilitating an adaptive ability to the dynamic deformation of the liquid balloon driven by the moving water waves. The dynamic self-adjust of the soft liquid balloon's shape can significantly increase the contact-separation area between the cotton layer and the inner surface of the hard acrylic spherical shell and facilitate the S-S triboelectric charge generation. Additionally, the exterior of the liquid balloon is coated with a cotton layer, serving as the counter-electrification layer. The entire balloon assembly is then securely mounted and suspended within the confines of the outermost hard spherical shell by a copper-core spring. This spring is integral to the LS-TENG, promoting an adaptive and responsive movement of the internal soft liquid balloon system relative to the rigid outer shell. The use of copper for the spring is due to its excellent electrical conductivity, mechanical strength, and, crucially, its elasticity, ensuring consistent performance under varying mechanical movements.

With respect to the binary immiscible liquid electrodes in the inner soft balloon, the combination of silicone oil and deionized water was employed. When these two immiscible phases were mechanically forced to mix caused by the working LS-TENG's swinging movements, plenty of transient generated dynamic L-L contact interfaces would be created, which significantly increases the L-L contact area, thereby increasing the triboelectric charges generated at the interface of the two phases. During the dynamic movement of the LS-TENG, the immiscible liquids (silicone oil and deionized water) within the soft liquid balloon are constantly in motion, leading to frequent contact and separation at their interfaces. This motion generates triboelectric charges due to the difference in electronegativity between the two liquids. As these two phases contact and then separate, a charge transfer occurs at the interface. The generated charges are not confined to the liquid interface but are transferred to the copper core spring, which is connected to the external circuit. This spring serves as a conductive pathway, allowing the charges to move from the liquid interface inside the soft liquid balloon to the external circuit. Once the triboelectric charges are transferred through the copper spring, they flow into the external circuit, contributing to the LS-TENG's electrical output. This continuous process of charge generation, accumulation, and transfer ensures efficient wave energy harvesting (Figure 1c).

Moreover, the unique self-adaptive and soft contact manner additionally increased the S-S contact area (Figure 1d), enhancing energy harvesting efficiency and protecting the LS-TENG device from mechanical wear and damage. Figure S3 exhibits the SEM images of the polyimide dielectric layer surface after different working periods (0 h, 6 h, 12 h, and 48 h), demonstrating little mechanical wear on the contact surfaces and effectively extending the TENG's working longevity. The unique structure of the LS-TENG provides an innovative and effective way of collecting wave energy.

2.2 The Working Principle of the LS-TENG: the Coupling of Dynamically Self-adjustable L-L Triboelectric Mechanism and S-S CE

Dynamically Self-adjustable L-L Contact Electrification (DSL-L CE). In the soft liquid balloon, silicone oil and deionized water are employed as binary liquid electrodes due to their immiscibility. Although these two liquids contact each other at their interface (Figure 2a-i), they remain separate as distinct bulk phases. Under the impetus of water waves, the LS-TENG's operation results in dynamic interactions within the inner liquid balloon, where the two immiscible liquids interpenetrate each other's bulk phases. As depicted in Figure 2a-ii, this interpenetration forms numerous temporary biphasic droplets of varying sizes and irregular shapes. As these droplets of the two liquids come into contact, their interfaces experience relative displacements, generating triboelectric charges through triboelectrification at these transient contact interfaces.

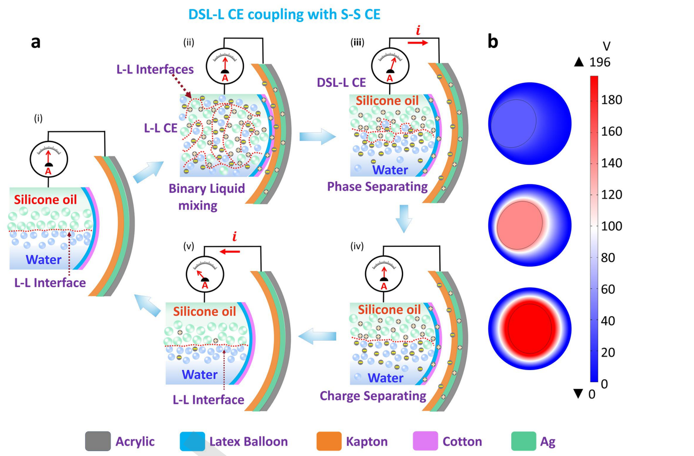

Figure 2. The overall coupling process of the DSL-L CE and the S-S CE. a) Formation mechanism of the dynamically self-adjustable L-L interfaces and the corresponding DSL-L CE coupling with the S-S CE. b) COMSOL Multiphysics simulation results showing the potential distribution across the LS-TENG during operation. The figure is color-coded to represent the voltage ranges, and the overall voltage gradient in the figure is 0-196 V.

Due to the inherent tendency of the immiscible phases to separate and return to their equilibrium positions, the charged droplets undergo dynamic migration (Figure 2a-(iii-v)), which makes the triboelectric charges dynamically transfer along the copper core spring to the external circuit [48]. The situation of the corresponding open-circuit voltage (VOC) is shown in Figure S4. By this means, an electric potential difference between the two liquid phases is generated. Thus, the corresponding ISC is generated. The L-L CE and dynamic self-adjustment of the L-L contact interfaces between these binary mixed liquid electrodes significantly enhance the charge transfer capabilities of the LS-TENG device, effectively improving its efficiency in harvesting and utilizing wave energy. Figure 2b illustrates the potential distribution of the LS-TENG during the LS-TENG's operation simulated by using COMSOL Multiphysics.

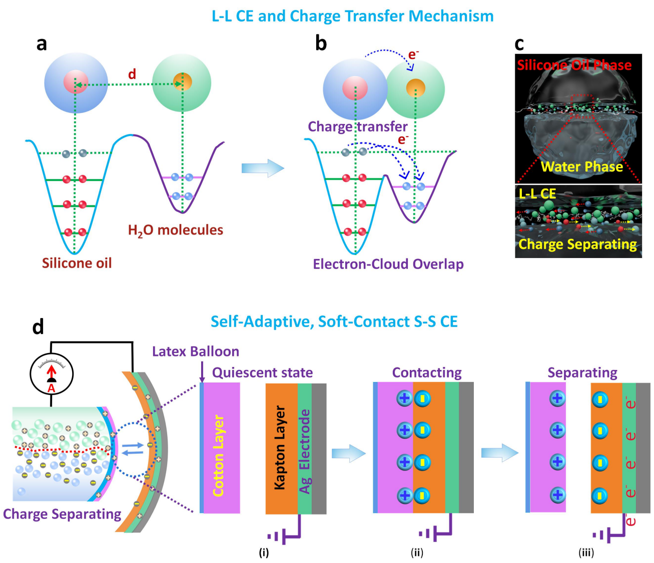

Figure 3. The charge transfer mechanism of the silicone oil-H_2O binary immiscible L-L interfaces and the S-S CE process between the self-adaptive

soft-contact interfaces (the cotton layer and the PI layer). a-b) The L-L CE and charge transfer mechanism based on the electron cloud potential-well model. a) Before the silicone oil-H_2O contacting. b) Contacting. c) The CE charges separate and migrate during the L-L interfaces' contacting and relative displacement occurring. d) The self-adaptive, soft-contact S-S CE process

The charge transfer mechanism at the dynamic L-L interface is illustrated in Figure 3a-b. Before the contact of the two liquid phases (Silicone Oil - H_2O molecules), the electrons could not transfer due to the local trapping effect of the potential wells (Figure 3a). When silicone oil contacts with H_2O molecules, the electron clouds overlap, and the initial single potential well of their own becomes asymmetric double-well potential and then the electrons could hop from the atom of silicone oil to the atom of H_2O molecules (Figure 3b). After hopping, the charges separate and migrate with the liquid phase moving (Figure 3c).

Self-adaptive and Soft Contact S-S Triboelectric Effect. Initially, without the push of external water waves, the liquid balloon is in a quiescent state (Figure 3d-i), retaining an ellipsoidal shape due to its gravity. However, when driven by the movement of water waves, the liquid balloon begins to swing back and forth, just like a moving pendulum, leading to the cotton layer repeatedly coming into contact (Figure 3d-ii) and separating (Figure 3d-iii) with the polyimide tape surface adhered to the inner surface of the hard acrylic spherical shell, and generating triboelectric charges at these two interfaces. During this dynamic process, the consequent real-time deformation of the soft liquid balloon appears. In an entire working cycle of the LS-TENG, self-adaptive and soft contact-separation processes occur alternatively between the polyimide tape adhered to the inner surface of the hard acrylic spherical shell and the cotton layer covered outside of the soft liquid balloon, significantly increasing the contact area compared with the traditional hard point contact manner, and consequently generating more triboelectric charges at the contact interfaces. Due to the periodic reciprocating movements of water wave energy, this self-adaptive and soft contact-separation mode proceeds also periodically. Moreover, this unique soft and self-adaptive contact-separation manner can significantly reduce mechanical wear and protect the LS-TENG from being structurally damaged caused by conventional hard point contact.

The coupling of the above DSL-L CE and the S-S CE. Based on the above discussion, here we propose a detailed DSL-L CE and the S-S CE coupling mechanism for the LS-TENG's working process: initially, the LS-TENG floats quietly on the surface of the water, with the soft liquid balloon suspended in the inner chamber of the hard acrylic spherical shell by the copper core spring. In this state, the liquid balloon could move along with the spherical shell. As we know, water waves provide both vertical lift and horizontal thrust movements due to the water particles' movement orbits in water waves. When a wave comes, the LS-TENG will be lifted and tilted by the buoyant force and water wave energy, making the inner liquid balloon convert the wave motion in the vertical direction into a lateral directional movement. As a water wave passes through the LS-TENG device, the mechanical energy of water waves could be transferred to the LS-TENG, causing the lateral displacement and tilt of the LS-TENG device. Consequently, when the water waves drive the whole LS-TENG, the liquid balloon swings laterally within the shell to repeatedly contact and separate with the inner surface of the hard acrylic spherical shell. By this means, the unique soft contact and self-adaptive manner is realized, significantly increasing the S-S contact area between the two electrification layers, thus enhancing the energy harvesting efficiency and protecting the LS-TENG device from mechanical wear and damage. During the LS-TENG's working process, both the S-S and the L-L CE couple to significantly enhance the wave energy harvesting efficiency of the LS-TENG's

2.3 The Influence of DSL-L CE on the LS-TENG's output performance.

To evaluate the L-L influence of the triboelectric effect generated between the binary immiscible liquid electrodes inside the latex balloon on the output performance of the LS-TENG, firstly, we selected silicone oil in combination with three distinct liquids as the LS-TENG's liquid electrode, respectively, including deionized water, ethylene glycol (EG), and glycerol (Gly), to form three pairs of binary immiscible liquid electrodes. The volume ratio of the silicone oil in each liquid pair is kept identical. The corresponding LS-TENG's output performances from each kind of binary immiscible liquid electrode were measured. The results show that the electric output performance of LS-TENG with the pair of silicone oil-deionized water as the liquid electrode is the best compared with those of the other two kinds of liquid pair electrodes, as shown in Figure 4a. To study the reason why the LS-TENG with silicone oil-deionized water liquid electrode pair exhibits the optimal electrical output performance, we further employ the silicone oil-deionized water pair as the liquid electrode with different volume ratios (0:1, 1:13, 1:1, 13:1, and 1:0) to test the LS-TENG's output performances. The result turns out that as the volume fraction of silicone oil in the binary mixture increases, the electrical output performance of the LS-TENG gradually boosts, including the V_{OC}, I_{SC}, and charge quantity (Q). However, this increasing trend does not persist all the time. As can be observed from Figure 4b, the optimal electrical output performance of the LS-TENG is achieved when the volume fraction of silicone oil reaches a 1:1 ratio. Subsequently, as the volume fraction of silicone oil continues to increase, the electrical output performance of the LS-TENG begins to decline.

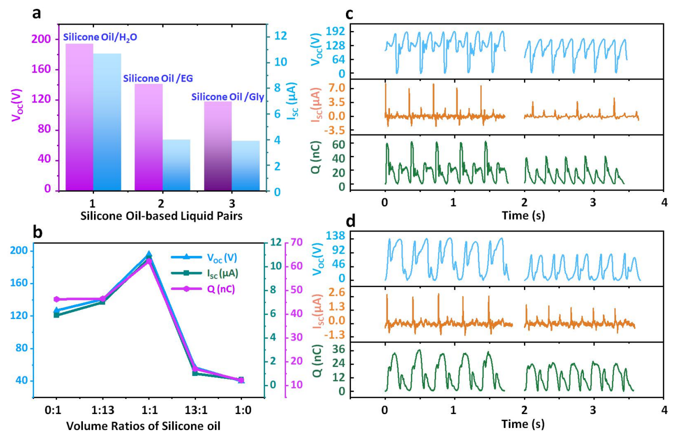

Figure 4. Further study and proof of the DSL-L CE mechanism. a) The LS-TENG's output performance comparison using different kinds of binary immiscible liquid pairs as the electrodes, including silicone oil-water, silicone oil-EG, and silicone oil-Gly. b) Optimizing the LS-TENG's output performance by using the silicone oil-water liquid pair as the electrode, in which the volume ratios of the silicone are 0:1, 1:13, 1:1, 13:1, and 1:0, respectively. c) The comparison of the LS-TENG's output performances, respectively, from the silicone oil-water pair (immiscible) and the Gly-water pair (miscible) as the liquid electrodes. d) The comparison of the LS-TENG's output performances, respectively, from the silicone oil-EG pair (immiscible) and the glycerin-ethylene glycol pair (miscible) as the liquid electrodes.

According to the above comparison results, one of the critical factors affecting LS-TENG's output performance should be attributed to the contact area between the two immiscible liquid phases. Compared to water, either ethylene glycol or glycerol forms a more cohesive mixture with silicone oil due to their inherently high viscosities, leading to the two phases being practically inseparable and unable to generate substantial dynamic separable L-L interfaces. In contrast, water is completely immiscible with silicone oil and has a lower viscosity. As a result, under the mechanical driving of ocean waves on the LS-TENG, a substantial number of temporary dynamic interfaces are formed between the silicone oil and water phases. These dynamic and self-adjustable L-L interfaces are continuously created and subsequently dissipated with the periodic mechanical driving of the water waves due to the natural phase separation of water and silicone oil. This constant process of contact and separation at these dynamic L-L interfaces generates triboelectric charges at the silicone oil and deionized water interfaces. Moreover, the significant difference in electrical conductivity between water and silicone oil leads to a potential difference between these interfaces upon their separation. According to the working mechanism of the contact-separating mode triboelectric nanogenerator, the triboelectric charges between the water and silicone oil interfaces are then transferred to the outer circuit, substantially enhancing the electrical output performance of the LS-TENG.

The 1:1 volume ratio of silicone oil to deionized water demonstrates the highest electrical output performance. The possible reason, we think, is that at 1:1 volume ratio of silicone oil to deionized water maximizes the contact area between the two immiscible liquids. At equal proportions, both liquids are able to form a balanced and widespread interface within the confined space of the LS-TENG's soft balloon. This balanced ratio allows both liquids to interact more extensively with each other, leading to the creation of numerous transient L-L interfaces as the balloon moves during operation. At other volume ratios (e.g., 1:3 or 3:1), one liquid dominates, reducing the effective contact area between the two phases. When one liquid occupies more space, the opportunities for interaction between the liquids are limited, leading to fewer dynamic L-L contact interfaces and, therefore, reduced triboelectric charge generation. In contrast, at the 1:1 ratio, the two immiscible liquids are evenly distributed, which maximizes their interaction as they repeatedly contact and separate. This increases the efficiency of the charge transfer process and enhances the overall electrical output performance of the LS-TENG. In essence, the 1:1 ratio optimizes the mechanical interaction and dynamic phase separation, ensuring a higher generation of triboelectric charges, which is why it results in better electrical output performance.

To confirm our proposed DSL-L CE mechanism, we further conducted a series of control experiments as follows. Four pairs of binary liquid electrodes were adopted, including (i) silicone oil-deionized water (Immiscible), (ii) glycerin-deionized water (Miscible), (iii) silicone oil-ethylene glycol (Immiscible), and (iv) glycerin-ethylene glycol (Miscible). As shown in Figure 4c, the left-side curves in this figure exhibit the LS-TENG's output performances from the silicone oil-deionized water pair as the liquid electrode (pair (i)), and the corresponding right-side curves show those of the glycerin-deionized water as the liquid electrode (pair (ii)). Similarly, the left side curves in Figure 4d give the LS-TENG's output performances from the silicone oil-ethylene glycol pair as the liquid electrode (pair (iii)), and the curves on its right side belong to those of the glycerin-ethylene glycol as the liquid electrode (pair (iv)). Obviously, the output performances shown on the left sides in Fig. 4c-d are all higher than those on the right sides, which means that the binary immiscible liquid electrodes endow the corresponding LS-TENG with better electric output performances than the binary miscible liquid electrodes do. Furthermore, the electric output performances of the LS-TENG from the silicone oil-deionized water pair (Immiscible) as the liquid electrode are better than those of the glycerin-deionized water pair (miscible) as the liquid electrode.

The results of these control experiments support the validity of the above-proposed DSL-L CE mechanism. Specifically, driven by the external water wave energy, the binary immiscible liquid electrodes within the LS-TENG form numerous dynamically self-adjustable L-L interfaces that significantly increase the L-L contact area of the LS-TENG, thus greatly enhancing the generation of triboelectric charges at the L-L interfaces. The formed transient, abundant dynamic L-L interfaces separate due to the phase separation of the immiscible liquid phases, thereby disrupting the symmetry of the positive and negative charges generated within the liquid electrodes. As a result, the generated positive and negative triboelectric charges do not neutralize each other due to geometric symmetry but are instead carried along with the L-L phase separation to the external circuit. This process effectively enhances the electrical output performance of the LS-TENG.

In contrast, in the binary miscible liquid electrode systems (such as pair (ii) and (iv)), where two liquids mix to form a uniform, stable single phase, no L-L interfaces are formed. Consequently, in the LS-TENGs utilizing these miscible binary liquids as electrodes, there is no generation of L-L interface triboelectricity, and the triboelectric charge generation occurs only through the S-S contact-separation between the external cotton layer covered on the soft liquid balloon and the inner surface of the external hard acrylic spherical shell. This feature distinguishes them significantly from systems where immiscible binary liquid electrodes create dynamic interfaces that enhance triboelectric effects.

2.4 Further Verification of the DSL-L CE and Optimization of the LS-TENG's Output Performance.

To further verify the dynamic triboelectric charge generation at the L-L interface of silicone oil-deionized water, we designed a validation experiment detailed in Figure 5a, in which we utilized a disposable infusion needle connecting with an infusion bottle to make the deionized water droplet fall downward to contact with the silicone oil layer covered on the bottom of the petri dish. By adjusting the roller on the infusion tube, the falling speed and frequency of the deionized water droplet could be controlled uniformly.

It's worth noting that a layer of copper tape was pre-attached to the bottom of the Petri dish as the electrode. The distance between the infusion needle and the surface of the silicone oil layer is precisely adjusted to ensure that each water droplet falling from the needle could be just in contact with the surface of the bottom silicone oil layer and, at the same time, does not break away from the tip of the needle. To avoid the previously fallen water droplets staying and directly spreading out on the surface of the silicone oil right below the tip of the needle, thus causing interference to the subsequent falling water droplets, the Petri dish is consequently inclined at a slight angle to allow each drop falling from the tip of the needle immediately to slide down the inclined silicone oil surface as soon as it touches the silicone oil surface.

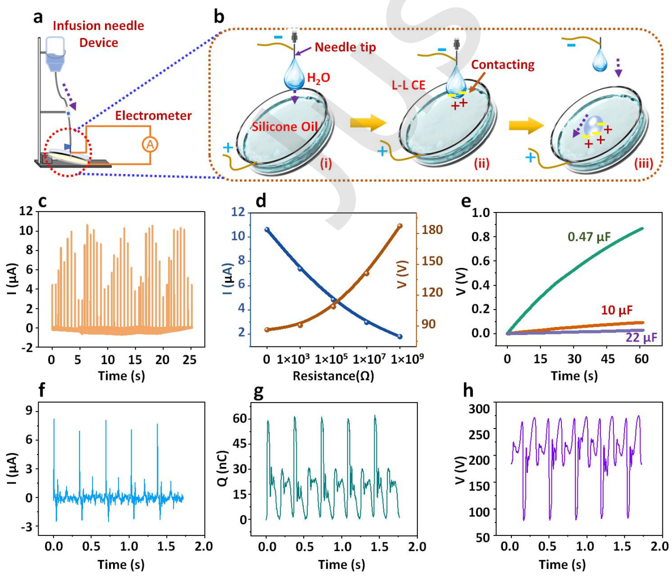

Figure 5. Further verify the dynamic triboelectric charge generation between the silicone oil-water L-L interfaces and optimize the LS-TENG's output performance. a) The dynamic triboelectric charge generation between the L-L interface of silicone oil-water. b) The L-L CE process at the L-L interfaces of the silicone oil-water. c) The dynamic triboelectric signal of L-L CE was detected. d) The optimal matching resistance is determined at the intersection of the two curves. e) The curves of charging different capacitors by using the LS-TENG. f-h) The maximum electric output performances: f) current (I), g) transfer charges (Q), and h). voltage (V).

By this method, a double-electrode mode TENG is constructed, as shown in Figure 5b. Once the water droplets from the tip of the needle come into contact with the surface of the silicone oil, an L-L CE occurs on their contact surfaces. In this continuous dynamic process, a potential difference is generated at the interface of silicone oil and water, and the corresponding voltage signals of the triboelectric effect are measured by connecting the positive and negative terminals of an electrostatic meter to the copper tape of the Petri dish and the needle, respectively, as depicted in Figure 5c. The result of this control experiment confirms our proposed DSL-L CE mechanism.

To enhance the conversion of mechanical energy into electrical energy by the LS-TENG and reduce energy losses during this process, we assess the impedance matching of the LS-TENG. As shown in Figure 5d, we connect resistors of varying values in series with the LS-TENG and record the current and voltage values with the values of the corresponding load resistance, and the optimal resistance is determined at the intersection of the two curves. Additionally, we tried to use the LS-TENG to charge capacitors of 0.47μF, 10μF, and 22μF, respectively. The corresponding charging curves are depicted in Figure 5e. Besides, the maximum output performances of the LS-TENG are obtained, shown in Figure 5 f-h.

2.5 All-weather and real-time monitoring for Marine IoT sensor

The marine environment, a complex and dynamic ecosystem, presents numerous hazards, especially due to its unpredictable weather conditions, such as storms, hurricanes, and strong currents that pose significant risks to operation at sea. To address these challenges, we have implemented real-time monitoring using all-weather sensors that can not only ensure the safety of operation at sea but also help marine meteorological analysis and forecasting. This sensing system tracks environmental parameters like temperature, humidity, and light intensity, with data visualized through a mobile app, as displayed in Video S1.

To realize marine environmental monitoring, the sensor systems employed typically operate on 3.7 V lithium batteries. However, due to the limited lifespan of these batteries, they require frequent replacements after certain periods of operation. This replacement process inevitably interrupts the sensor device's working, preventing continuous, real-time, all-weather monitoring. In this work, all-weather and real-time marine environment monitoring is achieved by continuously collecting ocean wave energy by the LS-TENG. The LS-TENG (Figure 6a) effectively charges the adopted lithium battery, which harnesses energy from ocean wave movements. By this means, the ocean wave energy is initially stored in the lithium battery and then converted into direct current (DC) to power the sensor system using a rectifier (Figure 6b), which not only powers the sensor system but also ensures a continuous and stable power supply under varying environmental conditions, as evidenced by the charging curve observed during the charging process (Figure 6c). Additionally, laboratory simulations of marine environments were conducted using linear motors to mimic ocean wave motions. These simulations facilitated optimizing the LS-TENG's performance by fine-tuning parameters such as speed and acceleration to closely match the natural frequencies of ocean waves, as demonstrated in Figure 6d and Video S2. For broader applications, the LS-TENG could be scaled up into a distributed network to increase energy harvesting capabilities from ocean wave movements (Figure 6e-f), ensuring the sensors' reliable operation across all weather conditions, as detailed in the equivalent circuit diagram shown in Figure 6g.

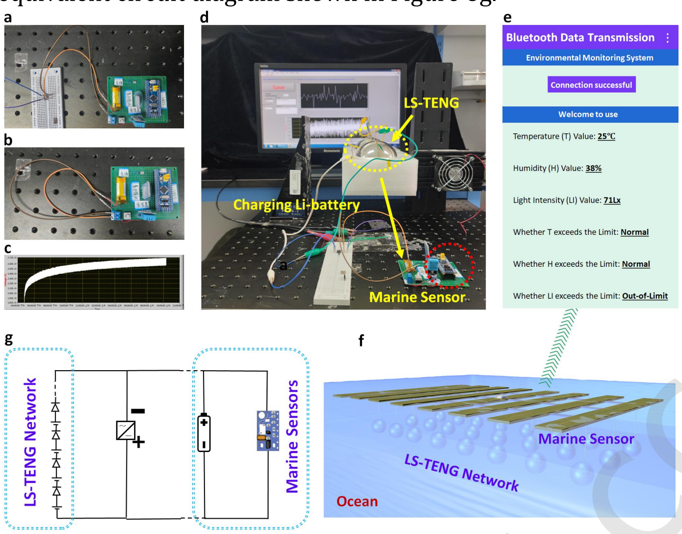

Figure 6. Powering the marine IoT sensor to realize all-weather and real-time monitoring for marine environmental monitoring. a) The lithium battery of the marine sensor is charged by the LS-TENG. b) The LS-TENG-charged lithium battery to power the marine sensor. c) The charging curve during the lithium battery charging process. d) Simulating marine environments to mimic ocean wave motions to optimize the LS-TENG's output performance. e-g) The schematic of the scaled-up LS-TENG into distributed networks to enhance energy harvesting capabilities from ocean waves: e) The mobile app showing the sensing results of the marine environmental monitoring. f) The schematic of the LS-TENG networks. g) The equivalent circuit diagram of the marine sensor powered by the LS-TENG.

3. Conclusion

In this work, an LS-TENG is designed to harvest water wave energy. The novel ellipsoidal, pendulum-like structure of the LS-TENG integrates both L-L and S-S triboelectric couplings. Firstly, the binary immiscible liquid electrodes in the inner soft balloon provide plenty of dynamic, self-adjustable L-L contact interfaces, significantly increasing the L-L contact area, thus enhancing the L-L CE and improving wave energy harvesting efficiency. Secondly, the unique self-adaptive, soft contact manner substantially increases the S-S contact area, which efficiently overcomes the limitation of the traditional solid-solid interface's point-point hard contact and makes the LS-TENG better adopt the irregular motions of water waves, not only enhancing the energy harvesting efficiency but protecting the TENG from mechanical wear and damage. The unique structure of the LS-TENG provides an innovative and effective way of collecting water wave energy. More importantly, the continuous marine environment sensor is successfully powered by the LS-TENG to realize all-weather and real-time marine environment monitoring, including temperature, humidity, and light intensity.

4. Experimental section

4.1 Fabrication of the Outer Hard Spherical Shell

First, two acrylic hemispherical shells with a diameter of 10 cm and a thickness of 0.21 cm are utilized. The clean inner shell is then uniformly coated with a silver layer by magnetron sputtering at 70W for 1200 s. Then, a polyimide film is carefully covered on the silver layer.

4.2 Preparation of the Inner Soft Liquid Balloon

A latex balloon, a polyurethane (PU) wrapped Cu-core spring, cotton, silicone oil, and deionized water were prepared. The binary immiscible silicone oil-water was injected into the latex balloon via a syringe. One end of the Cu-spring is inserted into the water phase of the liquid system of the balloon while its other end is led outside of the balloon. The liquid-filled balloon is then sealed, and a cotton layer is adhered to the balloon's exterior with a PVP solid adhesive.

4.3 LS-TENG's Assembly

A small hole slightly smaller than the Cu-spring's diameter is drilled into the prepared hard acrylic shell. The Cu-spring goes through the hole to the outside of the hard shell. Finally, the gaps between the Cu-spring and the hard shell are sealed via a hot melt adhesive (ethylene-vinyl acetate copolymer, EVA).

4.4 Measurement of output voltage and current:

To measure the triboelectric charge generation, we used the Keithley 6514, a high-precision electrometer, to capture the output voltage and current generated by the LS-TENG. The electrometer was connected to the external circuit of the LS-TENG, allowing real-time measurement of electrical output under different operational conditions, such as varying wave frequencies.

a) Voltage measurement: The electrometer was used to record the peak open-circuit voltage generated by the LS-TENG, ensuring accurate and consistent data collection. The high sensitivity of the electrometer allowed us to detect even small voltage fluctuations during operation.

b) Current measurement: Similarly, the electrometer measured the short-circuit current, which reflects the triboelectric charge transfer occurring between the L-L and S-S interfaces.

Acknowledgements

The authors acknowledge the financial support from the National Natural Science Foundation of China (Grant nos. 52173298, 52192611), the National Key R & D Project from Minister of Science and Technology (2021YFA1201603), Beijing Natural Science Foundation (Z230024), and the Fundamental Research Funds for the Central Universities.

Electronic Supplementary Material: Supplementary material (the optical image and the preparation of the LS-TENG device; the SEM images of the polyimide dielectric layer surface after different working periods, and the overall coupling process of the DSL-L CE and the S-S CE) is available in the online version of this article at https://doi.org/10.26599/NR.2025.94907052.

References

[1] Chen, B. D.; Tang, W.; He, C.; Deng, C. R.; Yang, L. J.; Zhu, L. P.; Chen, J.; Shao, J. J.; Liu, L.; Wang, Z. L. Water wave energy harvesting and self-powered liquid-surface fluctuation sensing based on bionic-jellyfish triboelectric nanogenerator. *Mater. Today* **2018**, *21*, 88-97.

[2] Yi, M.; Kong, W.; Zhang, Z.; Azam, A.; Ahmed, A.; Li, H.; He, L.; Li, N.; Xu, Y. A wave energy harvesting system for applications in deep-sea exploration. *Sustainable Energy & Fuels* **2023**, *7*, 1051-1066.

[3] Su, J.;Liu, Y.;Song, Y.;Huang, L.;Guo, W.;Cao, X.;Dou, Y.;Cheng, L.;Li, G.;Hu, Q.; Ye, R. Recent development of nanomaterials for carbon dioxide electroreduction. *SmartMat* 2022, 3, 35-53.

[4] Aster, R. C.; Ringler, A. T.; Anthony, R. E.; Lee, T. A. Increasing ocean wave energy observed in Earth's seismic wavefield since the late 20th century. *Nat. Commun.* **2023**, *14*, 6984.

[5] Kassayeva, A.; Balekova, A.; Yerzhanov, K. Converting the energy of sea waves into electrical energy. Environ. Prog. *Sustainable Energy* **2024**, *n/a*, e14342.

[6] Miao, X.; Yang, H.; Li, Z.; Cheng, M.; Zhao, Y.; Wan, L.; Yu, A.; Zhai, J. A columnar multi-layer sliding triboelectric nanogenerator for water wave energy harvesting independent of wave height and direction. *Nano Res.* **2024**, *17*, 3029-3034.

[7] Du, Y.; Tang, Q.; Fu, S.; Shan, C.; Zeng, Q.; Guo, H.; Hu, C. Chain-flip plate triboelectric nanogenerator arranged longitudinally under water for harvesting water wave energy. *Nano Res.* **2023**, *16*, 11900-11906.

[8] Howlader, T.; Farrok, O.; Kabir, M. A.; Abdullah-Al-Mamun, M.; Ali, M. S. Oceanic Wave Energy Devices. In Oceanic Wave Energy Conversion: Advancement of Electrical Generators. O. Farrok; M. R. Islam, Eds.; *Springer Nature Singapore; Singapore*, **2024**; pp 17-43.

[9] Xiong, C.;Wang, T.;Zhao, Z.; Ni, Y. Recent progress in the development of smart supercapacitors. *SmartMat* 2023, 4, e1158.

[10] Khan, U.; Kim, S.-W. Triboelectric Nanogenerators for Blue Energy Harvesting. *ACS Nano* **2016**, *10*, 6429-6432.

[11] Wang, Z. L. Triboelectric nanogenerators as new energy technology and self-powered sensors – Principles, problems and perspectives. *Faraday Discussions* **2014**, *176*, 447-458.

[12] Demircioglu, O.; Cicek, M. O.; Doganay, D.; Gazaloglu, G.; Baykal, C.; Cinar, S.; Unalan, H. E. Triboelectric nanogenerators for blue energy harvesting in simulated wave conditions. *Nano Energy* **2023**, *107*, 108157.

[13] Chen, H.; Xing, C.; Li, Y.; Wang, J.; Xu, Y. Triboelectric nanogenerators for a macro-scale blue energy harvesting and self-powered marine environmental monitoring system. *Sustainable Energy & Fuels* **2020**, *4*, 1063-1077.

[14] Wang, Y.; Wang, Y. Recent progress in MXene layers materials for supercapacitors: High-performance electrodes. *SmartMat* 2023, 4, e1130.

[15] Liang, X.; Jiang, T.; Feng, Y.; Lu, P.; An, J.; Wang, Z. L. Triboelectric Nanogenerator Network Integrated with Charge Excitation Circuit for Effective Water Wave Energy Harvesting. *Adv. Energy Mater.* **2020**, *10*, 2002123.

[16] Liang, X.; Liu, S.; Ren, Z.; Jiang, T.; Wang, Z. L. Self-Powered Intelligent Buoy Based on Triboelectric Nanogenerator for Water Level Alarming. *Adv. Funct. Mater.* **2022**, *32*, 2205313.

[17] Liang, X.; Liu, S.; Lin, S.; Yang, H.; Jiang, T.; Wang, Z. L. Liquid–Solid Triboelectric Nanogenerator Arrays Based on Dynamic Electric-Double-Layer for Harvesting Water Wave Energy. *Adv. Energy Mater.* **2023**, *13*, 2300571.

[18] Huang, B.; Wang, P.; Wang, L.; Yang, S.; Wu, D. Recent advances in ocean wave energy harvesting by triboelectric nanogenerator: An overview. *Nanotechnol. Rev.* **2020**, *9*, 716-735.

[19] Cao, C.; Li, Z.; Shen, F.; Zhang, Q.; Gong, Y.; Guo, H.; Peng, Y.; Wang, Z. L. Progress in techniques for improving the output performance of triboelectric nanogenerators. *Energy Environ. Sci.* **2024**, *17*, 885-924.

[20] Panda, S.; Hajra, S.; Oh, Y.; Oh, W.; Lee, J.; Shin, H.; Vivekananthan, V.; Yang, Y.; Mishra, Y. K.; Kim, H. J. Hybrid Nanogenerators for Ocean Energy Harvesting: Mechanisms, Designs, and Applications. *Small* **2023**, *19*, 2300847.

[21] Liu, L.; Yang, X.; Zhao, L.; Hong, H.; Cui, H.; Duan, J.; Yang, Q.; Tang, Q. Nodding Duck Structure Multi-track Directional Freestanding Triboelectric Nanogenerator toward Low-Frequency Ocean Wave Energy Harvesting. *ACS Nano* **2021**, *15*, 9412-9421.

[22] Zhao, X. J.; Wang, H. L.; Wang, Z. L.; Wang, J. Nanocomposite Electret Layer Improved Long-Term Stable Solid–Liquid Contact Triboelectric Nanogenerator for Water Wave Energy Harvesting. *Small* **2024**, *n/a*, 2310023.

[23] Meng, L.; Yang, Y.; Liu, S.; Wang, S.; Zhang, T.; Guo, X. Energy Storage Triboelectric Nanogenerator Based on Ratchet Mechanism for Random Ocean Energy Harvesting. *ACS Omega* **2023**, *8*, 1362-1368.

[24] Xu, L.; Jiang, T.; Lin, P.; Shao, J. J.; He, C.; Zhong, W.; Chen, X. Y.; Wang, Z. L. Coupled Triboelectric Nanogenerator Networks for Efficient Water Wave Energy Harvesting. *ACS Nano* **2018**, *12*, 1849-1858.

[25] Zhang, C.; He, L.; Zhou, L.; Yang, O.; Yuan, W.; Wei, X.; Liu, Y.; Lu, L.; Wang, J.; Wang, Z. L. Active resonance triboelectric nanogenerator for harvesting omnidirectional water-wave energy. *Joule* **2021**, *5*, 1613-1623.

[26] Gonçalves, I.; Rodrigues, C.; Ventura, J. Sea State Adaptation Enhances Power Output of Triboelectric Nanogenerators for Tailored Ocean Wave Energy Harvesting. *Adv. Energy Mater.* **2024**, *14*, 2302627.

[27] Yang, H.; Liang, X.; Kan, J.; Wang, Z. L.; Jiang, T.; Hong, Z. Triboelectric nanogenerator integrated with a simple controlled switch for regularized water wave energy harvesting. *Nano Res.* **2024**, *17*, 7585-7592.

[28] Yu, X.;Shang, Y.;Zheng, L.; Wang, K. Application of Nanogenerators in the Field of Acoustics. *ACS Appl. Electron. Mater.* **2023**, *5*, 5240-5248.

[29] Jiang, H.;Lv, X.; Wang, K. Application of triboelectric nanogenerator in self-powered motion detection devices: A review. *APL Mater.* **2024**, *12*.

[30] Pan, Y.;Zhu, Y.;Li, Y.;Liu, H.;Cong, Y.;Li, Q.; Wu, M. Homonuclear transition-metal dimers embedded monolayer C2N as promising anchoring and electrocatalytic materials for lithium-sulfur battery: First-principles calculations. *Appl. Surf. Sci.* **2023**, *610*, 155507.

[31] Sun, Z.;Yin, H.;Liu, K.;Cheng, S.;Li, G. K.;Kawi, S.;Zhao, H.;Jia, G.; Yin, Z. Machine learning accelerated calculation and design of electrocatalysts for CO_2 reduction. *SmartMat* **2022**, *3*, 68-83.

[32] Li, J.;Sun, Y.; Zhang, Z. Perspective on machine learning in energy material discovery. *SmartMat* **2023**, *4*, e1171.

[33] Yuan, Z.; Wang, C.; Xi, J.; Han, X.; Li, J.; Han, S.-T.; Gao, W.; Pan, C. Spherical Triboelectric Nanogenerator with Dense Point Contacts for Harvesting Multidirectional Water Wave and Vibration Energy. *ACS Energy Lett.* **2021**, *6*, 2809-2816.

[34] Liang, X.; Jiang, T.; Liu, G.; Feng, Y.; Zhang, C.; Wang, Z. L. Spherical triboelectric nanogenerator integrated with power management module for harvesting multidirectional water wave energy. *Energy Environ. Sci.* **2020**, *13*, 277-285.

[35] Liang, X.; Liu, Z.; Feng, Y.; Han, J.; Li, L.; An, J.; Chen, P.; Jiang, T.; Wang, Z. L. Spherical triboelectric nanogenerator based on spring-assisted swing structure for effective water wave energy harvesting. *Nano Energy* **2021**, *83*, 105836.

[36] Qu, Z.; Huang, M.; Chen, C.; An, Y.; Liu, H.; Zhang, Q.; Wang, X.; Liu, Y.;

Yin, W.; Li, X. Spherical Triboelectric Nanogenerator Based on Eccentric Structure for Omnidirectional Low Frequency Water Wave Energy Harvesting. *Adv. Funct. Mater.* **2022**, *32*, 2202048.

[37] Pang, Y.; Fang, Y.; Su, J.; Wang, H.; Tan, Y.; Cao, C. Soft Ball-Based Triboelectric–Electromagnetic Hybrid Nanogenerators for Wave Energy Harvesting. *Adv. Mater. Technol.* **2023**, *8*, 2201246.

[38] Xu, Z.; Chen, L.; Zhang, Z.; Han, J.; Chen, P.; Hong, Z.; Jiang, T.; Wang, Z. L. Durable Roller-Based Swing-Structured Triboelectric Nanogenerator for Water Wave Energy Harvesting. *Small* **2024**, *20*, 2307288.

[39] Rodrigues, C.; Nunes, D.; Clemente, D.; Mathias, N.; Correia, J. M.; Rosa-Santos, P.; Taveira-Pinto, F.; Morais, T.; Pereira, A.; Ventura, J. Emerging triboelectric nanogenerators for ocean wave energy harvesting: state of the art and future perspectives. *Energy Environ. Sci.* **2020**, *13*, 2657-2683.

[40] Wang, Y.; Liu, X.; Chen, T.; Wang, H.; Zhu, C.; Yu, H.; Song, L.; Pan, X.; Mi, J.; Lee, C.; Xu, M. An underwater flag-like triboelectric nanogenerator for harvesting ocean current energy under extremely low velocity condition. *Nano Energy* **2021**, *90*, 106503.

41] Gao, M.; Chen, Z.; Liang, J.; Lin, Z.; Zhou, Y.; Li, J.; Li, G.; Mo, L.; Shao, J.; Luo, Y. Self-Powered Buoy Triboelectric Nanogenerator with Nanofiber-Enhanced Surface for Efficient Wave Energy Harvesting. *ACS Appl. Polym. Mater.* **2023**, *5*, 5074-5081.

[42] Pang, H.; Feng, Y.; An, J.; Chen, P.; Han, J.; Jiang, T.; Wang, Z. L. Segmented Swing-Structured Fur-Based Triboelectric Nanogenerator for Harvesting Blue Energy toward Marine Environmental Applications. *Adv. Funct. Mater.* **2021**, *31*, 2106398.

[43] Jiang, T.; Pang, H.; An, J.; Lu, P.; Feng, Y.; Liang, X.; Zhong, W.; Wang, Z. L. Robust Swing-Structured Triboelectric Nanogenerator for Efficient Blue Energy Harvesting. *Adv. Energy Mater.* **2020**, *10*, 2000064.

[44] Xia, K.; Fu, J.; Xu, Z. Multiple-Frequency High-Output Triboelectric Nanogenerator Based on a Water Balloon for All-Weather Water Wave Energy Harvesting. *Adv. Energy Mater.* **2020**, *10*, 2000426.

[45] Feng, Y.; Jiang, T.; Liang, X.; An, J.; Wang, Z. L. Cylindrical triboelectric nanogenerator based on swing structure for efficient harvesting of ultra-low-frequency water wave energy. *Appl. Phys. Rev.* **2020**, *7*.

[46] Duan, Y.; Xu, H.; Liu, S.; Chen, P.; Wang, X.; Xu, L.; Jiang, T.; Wang, Z. L. Scalable rolling-structured triboelectric nanogenerator with high power density for water wave energy harvesting toward marine environmental monitoring. *Nano Res*. **2023**, *16*, 11646-11652.

[47] Shan, C.; He, W.; Wu, H.; Fu, S.; Li, K.; Liu, A.; Du, Y.; Wang, J.; Mu, Q.; Liu, B.; Xi, Y.; Hu, C. Dual Mode TENG with Self-Voltage Multiplying Circuit for Blue Energy Harvesting and Water Wave Monitoring. *Adv. Funct. Mater.* **2023**, *33*, 2305768.

[48] Lu, Y.; Jiang, L.; Yu, Y.; Wang, D.; Sun, W.; Liu, Y.; Yu, J.; Zhang, J.; Wang, K.; Hu, H.; Wang, X.; Ma, Q.; Wang, X. Liquid-liquid triboelectric nanogenerator based on the immiscible interface of an aqueous two-phase system. *Nat. Commun.* **2022**, *13*, 5316.

[49] Xu, Q.; Shang, C.; Ma, H.; Hong, Q.; Li, C.; Ding, S.; Xue, L.; Sun, X.; Pan, Y.; Sugahara, T.; Yalikun, Y.; Lai, Y.-C.; Yang, Y. A guided-liquid-based hybrid triboelectric nanogenerator for omnidirectional and high-performance ocean wave energy harvesting. *Nano Energy* **2023**, *109*, 108240.

Electronic Supplementary Material

Dynamically self-adjustable liquid-liquid and self-adaptive soft-contact solid-solid triboelectric nanogenerator for wave energy harvesting

Yong Long[1,2,§], Bingqi Zhao[2,3,§], Jianan Niu[2,3], Yuxiu Liu[2,3], Wei Sha[2,3], Jiangwen Wang[2,3], Zhong Lin Wang[1,2,3] (✉), and Weiguo Hu[1,2,3] (✉)

[1] *Guangzhou Institute of Blue Energy, Knowledge City, Huangpu District, Guangzhou 510555, China*
[2] *Beijing Institute of Nanoenergy and Nanosystems, Chinese Academy of Sciences, Beijing 101400, China*
[3] *School of Nanoscience and Technology, University of Chinese Academy of Sciences, Beijing 100049, China*
[§] *Yong Long and Bingqi Zhao contributed equally to this work.*

Supporting information to https://doi.org/10.26599/NR.2025.94907052

Figure S1. The optical image of the LS-TENG device.

Address correspondence to Weiguo Hu, huweiguo@binn.cas.cn; Zhong Lin Wang, zlwang@binn.cas.cn

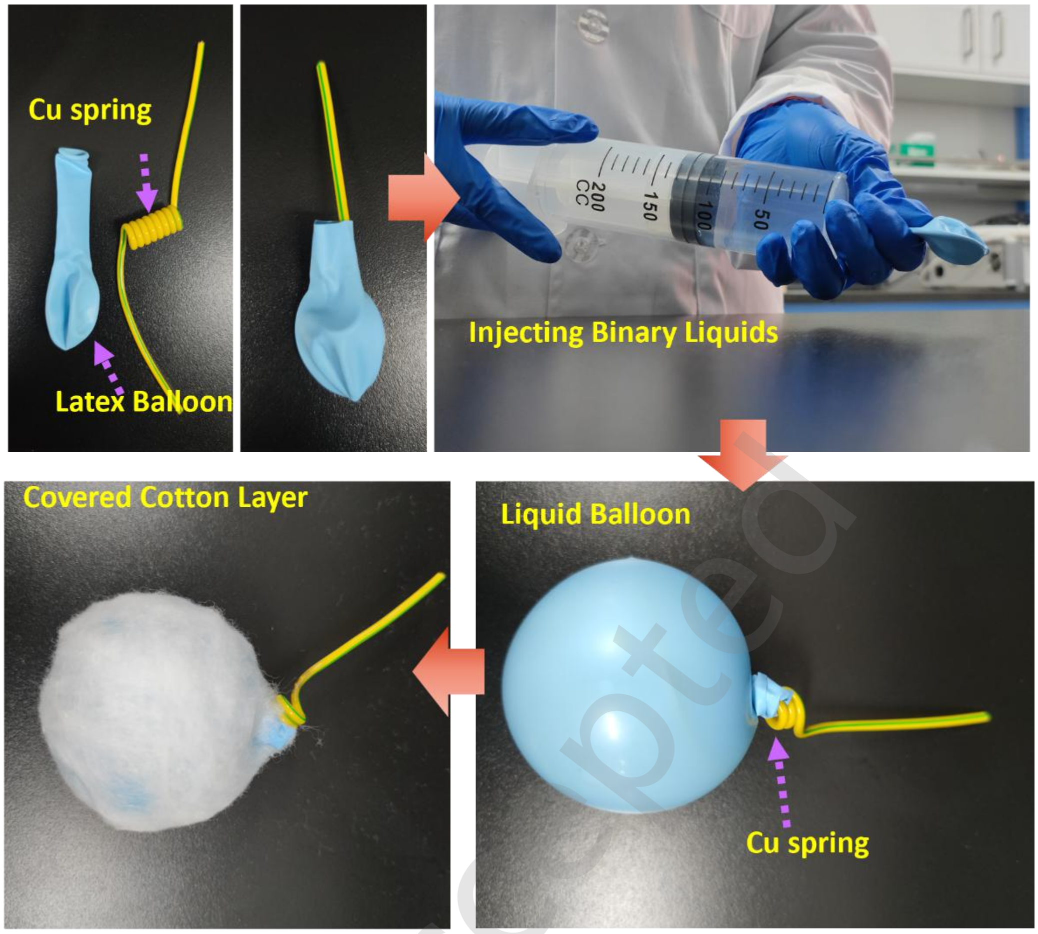

Figure S2. The preparation process of the internal soft liquid balloon of the LS-TENG.

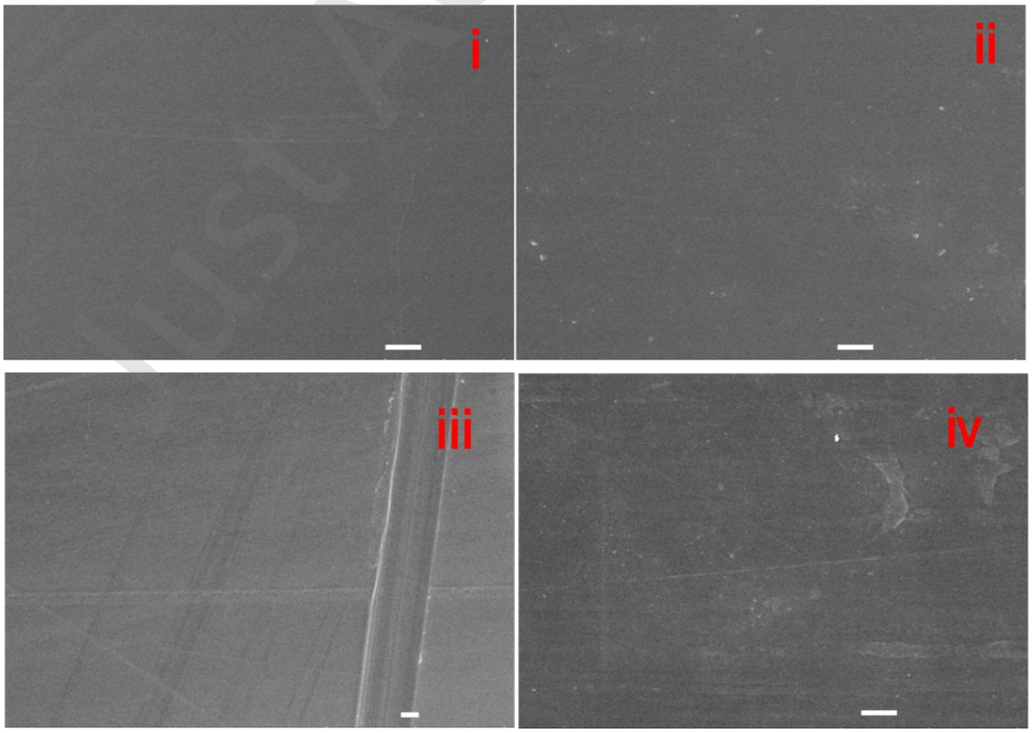

Figure S3. SEM images of the polyimide dielectric layer surface after different working periods (0 h, 6 h, 12 h, and 48 h), demonstrating little mechanical wear on the contact surfaces and effectively extending the TENG's working longevity.

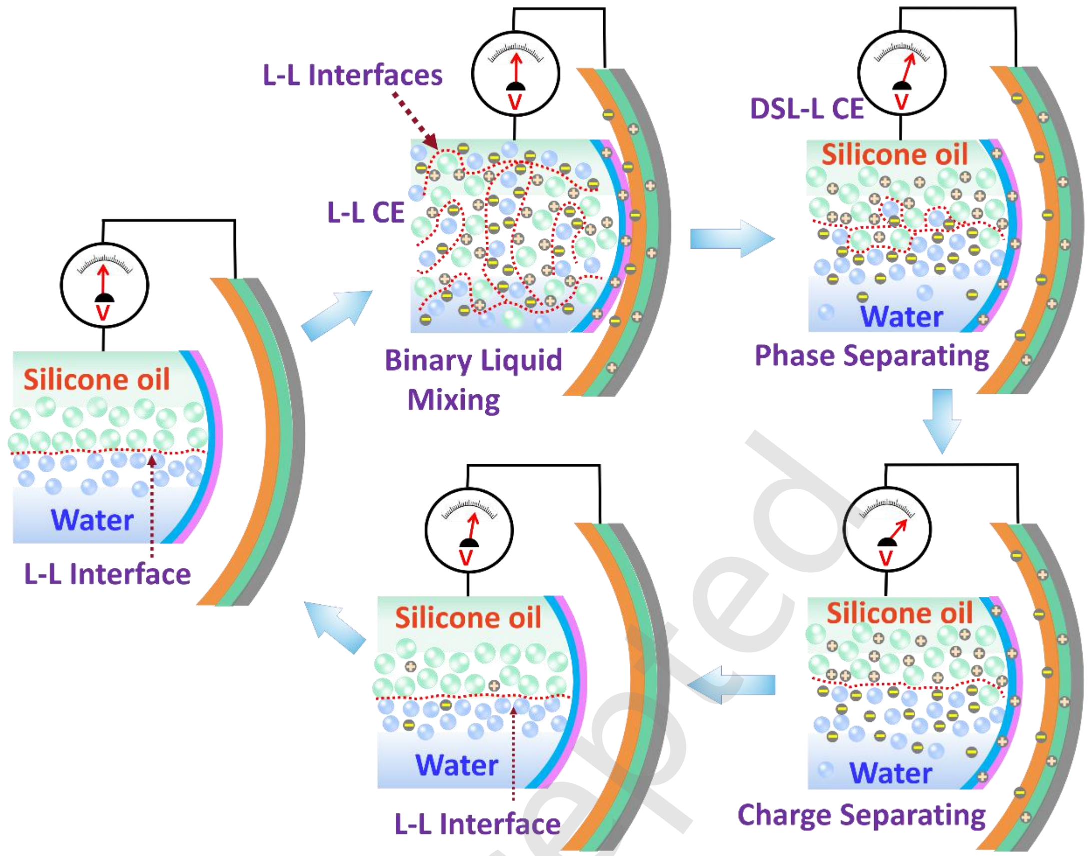

Figure S4. The overall coupling process of the DSL-L CE and the S-S CE. a) The output performance of Voc of the LS-TENG during the DSL-L CE and coupling with the S-S CE.